REPORT DOCUMENTATION PAGE

Form Approved
OMB No. 0704-0188

1. REPORT DATE *(DD-MM-YYYY)*	2. REPORT TYPE	3. DATES COVERED *(From - To)*
03/29/2016	Final/EOY	Sept 1 2012 - Aug 31 2015

4. TITLE AND SUBTITLE
Electrolyte Transport in Confined Spaces

5a. CONTRACT NUMBER

5b. GRANT NUMBER
N000141211021

5c. PROGRAM ELEMENT NUMBER

6. AUTHOR(S)
White, Henry S.
Voth, Gregory A.

5d. PROJECT NUMBER

5e. TASK NUMBER

5f. WORK UNIT NUMBER

7. PERFORMING ORGANIZATION NAME(S) AND ADDRESS(ES)
Dept of Chemistry, University of Utah, 315 S. 1400 E., Salt Lake City, UT 84112
Dept of Chemistry, The University of Chicago, 5735 S. Ellis Ave, Chicago, IL 60637

8. PERFORMING ORGANIZATION REPORT NUMBER

9. SPONSORING/MONITORING AGENCY NAME(S) AND ADDRESS(ES)
Office of Naval Research
875 North Randolph Street
Arlington, TX 22203-1995

10. SPONSOR/MONITOR'S ACRONYM(S)
ONR

11. SPONSOR/MONITOR'S REPORT NUMBER(S)

12. DISTRIBUTION/AVAILABILITY STATEMENT
unlimited, nonconfidential

13. SUPPLEMENTARY NOTES

14. ABSTRACT

We report research into the fundamentals of charge transport in confined electrolyte systems that are of fundamental and technological importance in energy-storage systems and in the development of nanoscale electrochemical platforms, including new chemical and physical sensors. Experimental studies quantifying the role of electrical field driven ion transport in electrolytes that are 10s of nm thick, including at the 3-phase interface, are reported. Descriptions and results from multiscale computational modeling of charge transport in nanoscale electrochemical devices involving specialized large-scale molecular dynamics simulations and novel coarse-graining methods are presented.

15. SUBJECT TERMS
Electrochemistry; coulomb transport; battery; nonequilibrium multi-scale computational methods; Kinetic Monte Carlo – Molecular Dynamics simulation; nanofabrication; electrical double layer; thin-layer electrochemical cells.

16. SECURITY CLASSIFICATION OF:			17. LIMITATION OF ABSTRACT	18. NUMBER OF PAGES	19a. NAME OF RESPONSIBLE PERSON
a. REPORT	b. ABSTRACT	c. THIS PAGE			Henry S. White
					19b. TELEPHONE NUMBER *(Include area code)*
U	U	U	UU	19	801-585-6256

Report Information

Name: Henry S White
Organization: University of Utah
Email: white@chem.utah.edu

Contract Information
Contract Number: N000141211021
Contract Title: Electrolyte Transport in Confined Spaces
Program Officer: Michele Anderson
CO-PI Information: Gregory A Voth – University of Chicago

Abstract
We report research into the fundamentals of charge transport in confined electrolyte systems that are of fundamental and technological importance in energy-storage systems and in the development of nanoscale electrochemical platforms, including new chemical and physical sensors. Experimental studies quantifying the role of electrical field driven ion transport in electrolytes that are 10s of nm thick, including at the 3-phase interface, are reported. Descriptions and results from multiscale computational modeling of charge transport in nanoscale electrochemical devices involving specialized large-scale molecular dynamics simulations and novel coarse-graining methods are presented.

TECHNICAL SECTION

TECHNICAL OBJECTIVES

The focus of this research is concerned with the fundamentals of charge transport in confined electrolyte systems, as well as with the design of novel nanofluidic cells for electrochemical research that are of fundamental and technological importance in energy-storage systems and in the development of nanoscale electrochemical platforms, including new chemical and physical sensors. Experimental studies are aimed at quantifying the role of electrical field driven ion transport in electrolytes that have thicknesses of 10s of nanometers and are confined by charged electrochemical interfaces. Multiscale computational methods need to be developed and applied for the modeling of charge transport in nanoscale electrochemical devices. These methods will involve specialized large-scale molecular dynamics simulations and the use of novel coarse-graining methods to connect the molecular-scale dynamics to transport equations under nonequilibrium conditions beyond the reach of the traditional simulation approaches. Additionally, we propose to extend these basic studies to electrochemical cells based on chemistries of technological interest.

TECHNICAL APPROACH

Simulations using multi-scale computational models have been performed to investigate the fundamental properties of ion transport within nano-confined electrolytes under applied voltages. These simulations offer new insights about the design of the devices related to energy storage and generation. In the Voth group, the new multi-scale computational methods have been implemented within the reactive molecular dynamics (RMD) simulation framework. This advanced model has been applied for systematic simulations of different types of ion transport in nano-scale electrochemical devices, such as hydrated proton solvation and transport near electrodes [J. Phys. Chem. C **119,** 14675–14682 (2015)], transport of the redox couple ($[IrCl_6]^{2-/3-}$) in aqueous solution, and transport of charged cluster $[Mg_xTFSI_y]^{(2x-y)+}$ in non-aqueous

acetonitrile solution [J. Phys. Chem. B 119, 7516–7521 (2015)]. These results are useful to understand the concept of the "Coulomb transport" (CT) effect, proposing applications for these effects, and adjusting these effects in prototypical systems. The methodology development and large-scale computational simulations performed in the Voth group have created a predictive multiscale computational framework to aid in the design of novel energy storage and have provided insights at the atomistic level for the design of devices such as multi-dimensional batteries and nano-scale fuel cells.

On the experimental side, the White group has designed and fabricated nanofluidic electrochemical cells (nFEC) that have electrode separation dimensions on the order of tens of nanometers. The Au/electrolyte/Au cell structures allow study of charge and molecular transport with focus on the influence of charged interfaces on current densities achievable between closely spaced electrodes. In the past year, we have used nanogap electrochemical cells to study the aqueous redox couple $Ru(NH_3)_6^{2/3+}$ due to its very high ionic charge, in contrast to the previous non-aqueous Fc/Fc^+ experiments, to challenge our recent predictions of electric field driven transport in high electric fields. The current-voltage relationship of these cells is being measured as a function of the cell thickness and electrolyte concentration to determine when high-field transport becomes operative. An additional opportunity to study ion and electron transfer in a highly confined system occurs at the circumference of electrochemically generated gas nanobubbles (< 50 nm radius) at Pt nanodisk electrodes. These systems provide a unique platform to quantify ion/electron-transfer reaction kinetics at 3-phase gas/liquid/solid interfaces that are fundamental to electrochemical energy storage systems. This past year, we have extended these measurements to investigate the gas molecule transport rates across the nanobubble/electrolyte interface and the dependence of surface tension (Laplace pressure) on bubble size for H_2 bubbles of radius between 10 and 50 nm.

Progress Statement

PROGRESS STATEMENT SUMMARY

Key progress has been made to implement the efficient yet accurate electrode-electrolyte model based on the method of images, as well as the constant voltage applied through the cell, into the multi-configurational reactive molecular dynamics (RMD) framework, thus enabling us to model the ion transport within the nanometer cell in a realistic manner. In the past funding period this approach was used to study ion transport at nanometer cell dimensions and high fields. The prediction of CT was confirmed by carrying out atomistic simulations of a prototypical electrochemical cell. With the newly developed reactive electrode-electrolyte formalism, we have performed in-depth investigations of ion transport under the influence of the CT effect and we have proposed ways to adjust/apply this effect into the design of energy storage related devices.

Experimentally, the voltammetric responses of thin-layer electrochemical cells with thicknesses less that 100 nm have been demonstrated to be in excellent agreement with predictions of the effects of electric double layers on ion transport. Specifically, we have shown that cell currents are reduced to negligible values when an insufficient number of electrolyte ions are present to

shield the electrode surface charge. New experimental studies this year using the $Ru(NH_3)_6^{2/3+}$ redox couple demonstrated that the positive anode potential creates an electrostatic barrier repels $Ru(NH_3)_6^{2+}$ from reaching the anode and causing the dramatic current decrease in current flow. The results are in excellent agreement with predictions of coupled ion transport and high electric fields in the constrained thin-layer electrochemical cell. In related experiments, the *first ever* measurements of electron transfer at a single gas/liquid/solid electrode interface have been performed. In recent work, we reported the *lifetimes* of individual H_2 and N_2 nanobubbles, electrochemically generated at Pt nanoelectrodes (7 to 85 nm radius), measured using a newly developed fast-scan electrochemical technique. These experiments provide the first direct measurement of interfacial gas-transfer kinetic rates for bubbles less than 100 nm in size, and provide a crucial test for existing theories governing bubble dissolution. We also constructed a novel pressure chamber to directly measure the Laplace pressure of electrochemically generated nanobubbles as small as 10 nm in radius, to directly test thermodynamic relationships at nanometer length scales. These are key fundamental parameters in electrochemical technologies that have never been previously evaluated.

PROGRESS

The Voth group has focused on modeling and simulating of ion transport through electrolytes related to energy storage and applications. Understanding and predicting ion transport properties under the CT effect require the development of the realistic model, which can efficiently yet accurately present electrode-electrolyte interactions. Such requirements have been accomplished by implementing the polarizable electrode model based on the image charge method into the reactive molecular dynamics (RMD) simulations, and thus enable us to model the more complex ion transport process in a realistic manner. As a continuation of the past funding period, these computational simulations provide deeper understanding about the CT effect and explore the ways to apply this effect into the electrochemical cells.

With the constant applied potential model of electrode-electrolyte framework in place, we first shifted our focus to a more complex problem: the study of proton transport in electrochemical cells driven by external applied voltages in aqueous electrolytes (Fig. 1). This is a particularly challenging problem because the hydrated proton charge defect can delocalize over several solvation shells, while the transport of this charge defect leads to collective behavior of the related water molecules, thus requiring the use of a RMD model that allows for changes in bonding topology. Previously in the Voth group multi-configuration reactive models have been developed and implemented into the LAMMPS package, as an in-house code named RAPTOR. Incorporating the constant potential electrode-electrolyte framework into RAPTOR, a non-trivial task, has been accomplished to study the proton transport under applied voltages. The long-range electrode-electrolyte interactions are presented using the particle-particle-particle mesh (PPPM) method together with the symmetry of the image charges. The van der Waals (vdW) interactions between the hydronium cation and electrode atoms are fitted from the *ab initio* calculations, while the water-electrode. vdW interaction parameters are obtained from the work of the Siepmann group [J. Chem. Phys. 102, 511, (1995)] .

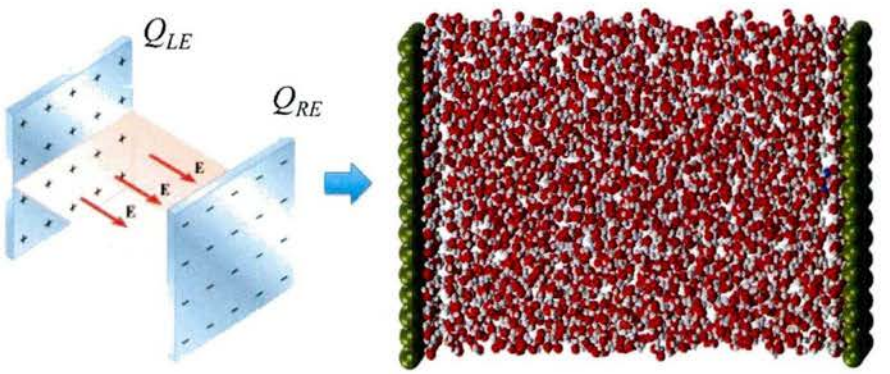

***Figure 1**: Schematic view of image charge method and a snapshot of the simulation of proton transport under applied voltages.*

Hydrated Proton Solvation and Transport at Electrodes under External Applied Voltages

Using the above RMD framework, we have modeled hydrated proton solvation and transport in a prototypical energy storage system that consists of an aqueous electrolyte held between metal electrodes with an applied external voltage [J. Phys. Chem. C **119,** 14675–14682 (2015)]. The simulations incorporate the multi-configurational RMD approach to model proton transport including Grotthuss shuttling mechanism as well as an accurate, physically motivated representation of the electrode–electrolyte interaction. Water-mediated hydrated proton solvation and diffusion at two types of platinum-water interfaces–namely, the Pt(111) and the Pt(100) surfaces–were investigated using the RMD simulation. The adsorbed water molecules on these platinum surfaces create different hydrogen-bonding networks, resulting in different proton solvation and transport behavior. Free energy calculations (see Fig. 2) show that the excess proton can be stably adsorbed on the Pt(111) surface, while on the Pt(100) surface it prefers to stay at the interface between the hydrophobic layer of adsorbed water and the bulk. The hydrated excess proton can be viewed as a charge defect in the adsorbed water layer, where it diffuses with a low rate due to the slow reorientational dynamics of the adsorbed water molecules. However, the proton can sample a larger surface area by hopping between the adsorbed layer and the bulk at the Pt(111) surface.

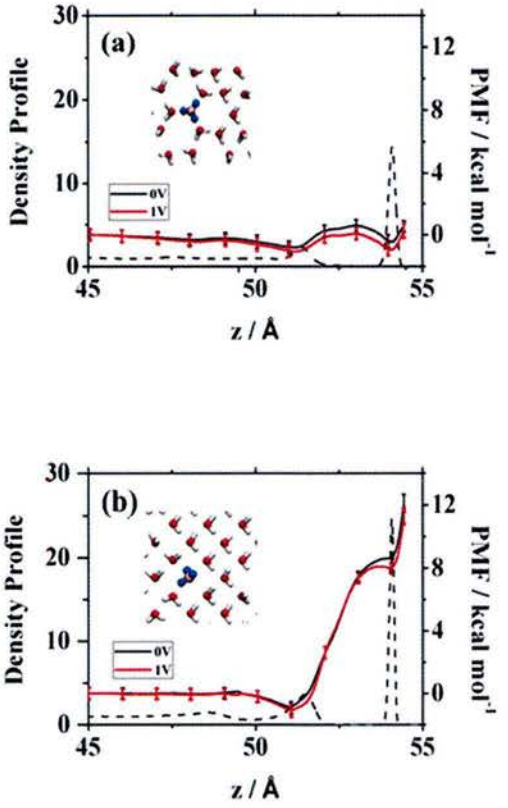

Figure 2: Free energy (with error bars) as a function of the distance, in the z-direction (namely the axis perpendicular to the electrode surface), of the hydrated excess proton center of excess charge (CEC) from the positive electrode at two different voltages (0V and 1V) for: (a) Pt(111) surface, and (b) Pt(100) surface. The inset in each graph is a snapshot of the local environment of the hydronium surrounded by the water molecules adsorbed on the corresponding Pt surface. The black dashed line shows the water density.

Ion Transport through Ultrathin Electrolyte under Applied Voltages

To further investigate the influence of the CT effect on ion transport, as well as to modify and apply such effects, two additional systems were constructed and simulations were performed to build solid foundations for the real applications of this effect to the energy storage devices [J. Phys. Chem. B 119, 7516–7521 (2015)]. The first system consists of the $[IrCl_6]^{2-/3-}$ redox couple in ultra-thin aqueous electrolyte between platinum electrodes. In this prototypical electrochemical cell, the diffusion of the $[IrCl_6]^{3-}$ anion against the electric field toward the negative electrode is essential to generate the current. However, the ultra-thin electrolyte cannot fully shield the applied electric field, and the unscreened electric field (CT effect) can trap the anions near the positive electrode and decrease the redox reaction rate by lowering the number of anions surrounding the negative electrode. Considering the origin of the CT effect, a straightforward way to modify this effect and enhance the efficiency of the electrochemical cell is to add supporting charges into the electrolyte to assist in shielding the

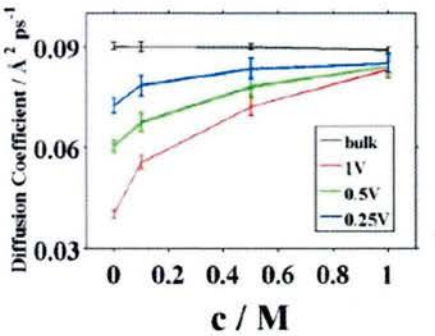

Figure 3: *Effective diffusion constants of the redox couple in aqueous solution with 0, 0.1, 0.5 and 1M supporting charges under 0.25, 0.5 and 1V applied voltages. The bulk value is also shown as a benchmark.*

electric field. To validate these expectations, the simulations were performed and the transport behavior of the redox couple under a range of applied voltages as well as different concentrations of supporting charges have been explored (Fig. 3). As expected, the results show that the diffusion of the anions are inhibited by the CT effect, while adding supporting charges can mitigated this effect and enhance the charge transport in this ultra-thin aqueous electrolyte (Fig. 4). The study also proposed the ways to validate these simulation results through cyclic-voltammetry experiments, and the influences of the CT effects can be observed as the peak value in those *i-V* curves.

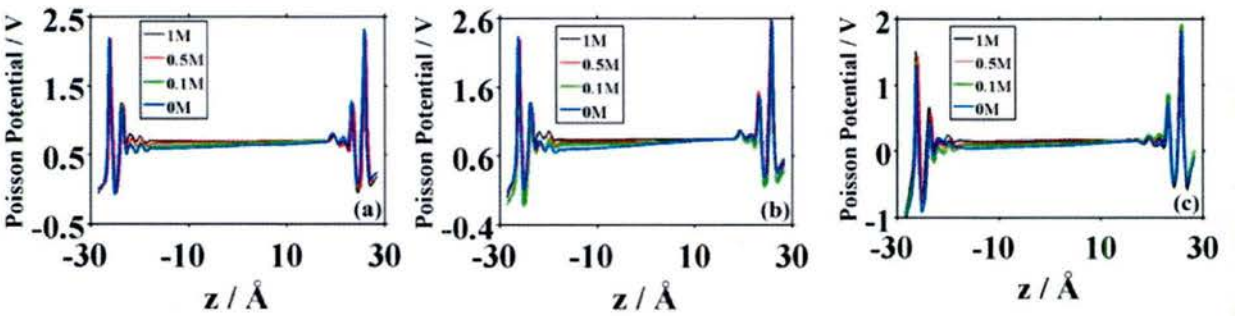

***Figure 4**: Poisson potential drop through the electrolyte under (a) 0.25V, (b) 0.5V, and (c) 1V applied voltages.*

The second prototypical system is chosen as the $Mg[TFSI]_2$ in acetonitrile solution under a range of applied voltages. An interesting behavior for this specific system is that the Mg^{2+} cation tends to form clusters with the $TFSI^-$ anion (Fig. 5). Due to their lowered charge density as compared to Mg^{2+} cations, Mg^{2+} clusters do not support efficient charge transport. The CT effect may provide an unscreened electric field, which will drive Mg^{2+} cations and $TFSI^-$ anions in opposite directions, helping to separate the clusters and therefore enhance the charge transport efficiency in the electrolyte. The simulations results support these expectations, that the CT effect leads to opposite direction forces acting on the cations and anions, and this effect may be applied to help break the clusters and therefore enhance the electrochemical cell efficiency. Together, the studies have explored the ways to adjust the CT effect and proposed further applications of the effect in the real systems related to the nano-scale energy storage devices.

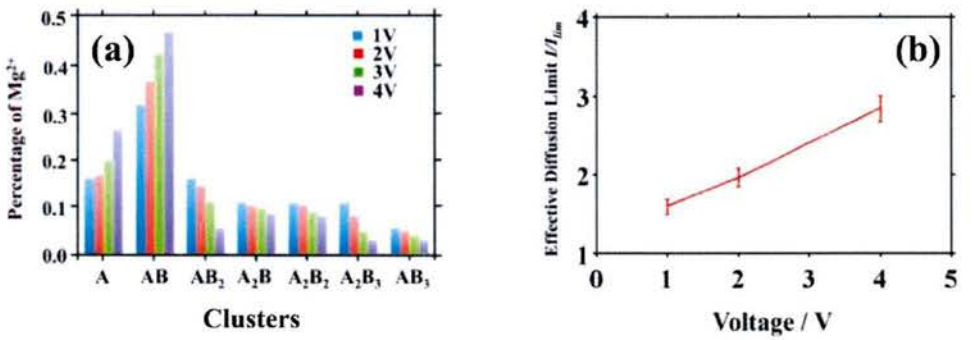

***Figure 5**: (a) Distribution of the Mg^{2+} forming different sizes of $[Mg_x(TFSI)_y]^{(2x-y)+}$ clusters in acetonitrile electrolyte at different applied voltages. A represents Mg^{2+}, and B represents $TFSI^-$ in the figure.*

Experimental Studies of Electric Double Layer Effects in Nanometer-Wide Thin-Layer Cells

Ion Transport in the Double Layer Overlap Regime of Nanometric-Thin -Layer Electrochemical Cells.

In the 2014 EOY report, we detailed the fabrication and characterization of nanogap electrochemical cells, which consist of two 20 micron diameter disk electrodes separated by gaps from 40 to 400 nm [*ACS Nano* 2015, *9*, 8520] (Figure 6). Because of the close spacing between the two planar electrodes, redox species generated at one electrode can be collected at the other electrode, with near 100% efficiency and a significant current enhancement may be achieved through redox cycling (repeated oxidation and reduction of a single redox molecule at closely spaced electrodes). We showed that for the Fc/Fc^+ redox couple (Fc = ferrocene) in acetonitrile, that lowering the supporting electrolyte concentration resulted in significant attenuation in the steady-state voltammetric current. An explanation was provided through finite element modelling of the coupled mass-transport, electric fields and electron transfer kinetics. The underlying theory of the coupling of double-layer fields with modern electron-transfer rate theory was detailed in our *ACS Nano* **2014**, *8*, 10426 article.

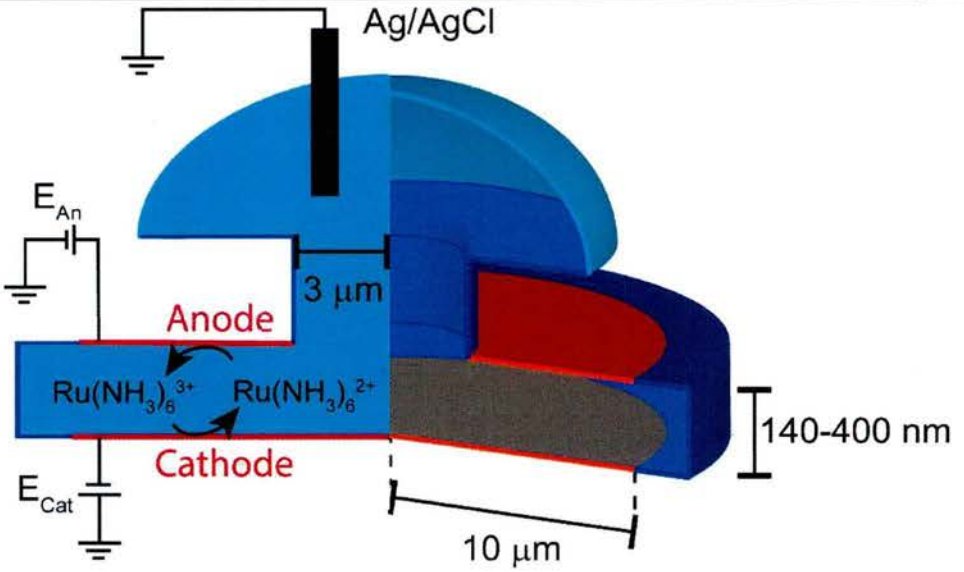

Figure 6. Schematic of the nanogap electrochemical cell and the redox cycling of $Ru(NH_3)_6^{3/2+}$ with relevant dimensions labelled (not to scale).

Understanding of electric double layers and ion transport near interfaces is of fundamental importance in a variety of applications, ranging from electrochemistry and electrophoresis, to nanofluidics and water desalination. Nanoscale ion transport occurs in a range of high performance electrochemical energy systems, such as fuel cells, batteries, and supercapacitors. A fundamental understanding of transport within double layer and in confined geometries is important in the quest for improved energy and power densities.

Since the previous reporting period we have used nanogap electrochemical cells to study the aqueous redox couple $Ru(NH_3)_6^{2/3+}$ which undergoes redox cycling as shown schematically in the left hand side of Figure 6. We chose the $Ru(NH_3)_6^{2/3+}$ couple due to its high ion charge, in contrast to Fc/Fc^+, to challenge our recent predictions of electric field driven transport in high electric fields. In remarkable contrast to the Fc/Fc^+ couple in acetonitrile, we observed enhancement of the experimental voltammetric current as the supporting electrolyte concentration was lowered, as is shown in Figure 7 parts a and c (experimental, two different cell thicknesses). Moreover, the voltammograms show a plateau in contrast to the peaked shape previously observed. An enhanced current is of interest in sensing applications, which, as in this work, are most typically performed in aqueous environments.

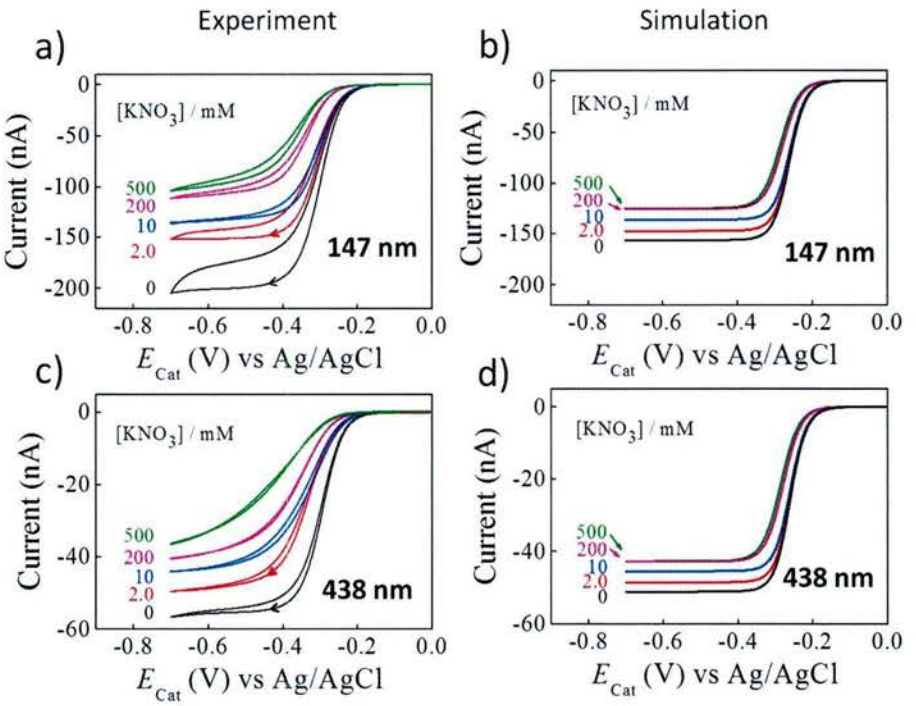

Figure 7. Experimental (a, c) and simulated (b, d) voltammetric responses of 1.0 mM $Ru(NH_3)_6Cl_3$ in H_2O with KNO_3 concentrations as labeled. Cell thicknesses were (a, b) 147 nm, and (c, d) 438 nm. The scan rate was 10 mV/s. Arrows indicate the forward potential scan. $E_{An} = 0$ V.

Figure 7, parts c and d, show voltammograms computed from finite element simulations of the system (coupled mass-transport, electric fields and electron transfer kinetics). The same current trends are observed as in the experimental system. An explanation of the current enhancement is provided by inspection of the resultant concentration and potential distributions. These are shown in Figure 8, which shows the distribution at the switching potential (E_{Cat} = -0.7 V) for excess (500 mM) and no supporting electrolyte. While the $Ru(NH_3)_6^{3+}$ concentration is comparable for both cases (part c) there is a dramatic enhancement of the $Ru(NH_3)_6^{2+}$ concentration on the cathode surface as is shown in part d. The enhancement is due to electrostatic interactions that are reflected in the potential distribution (part b)

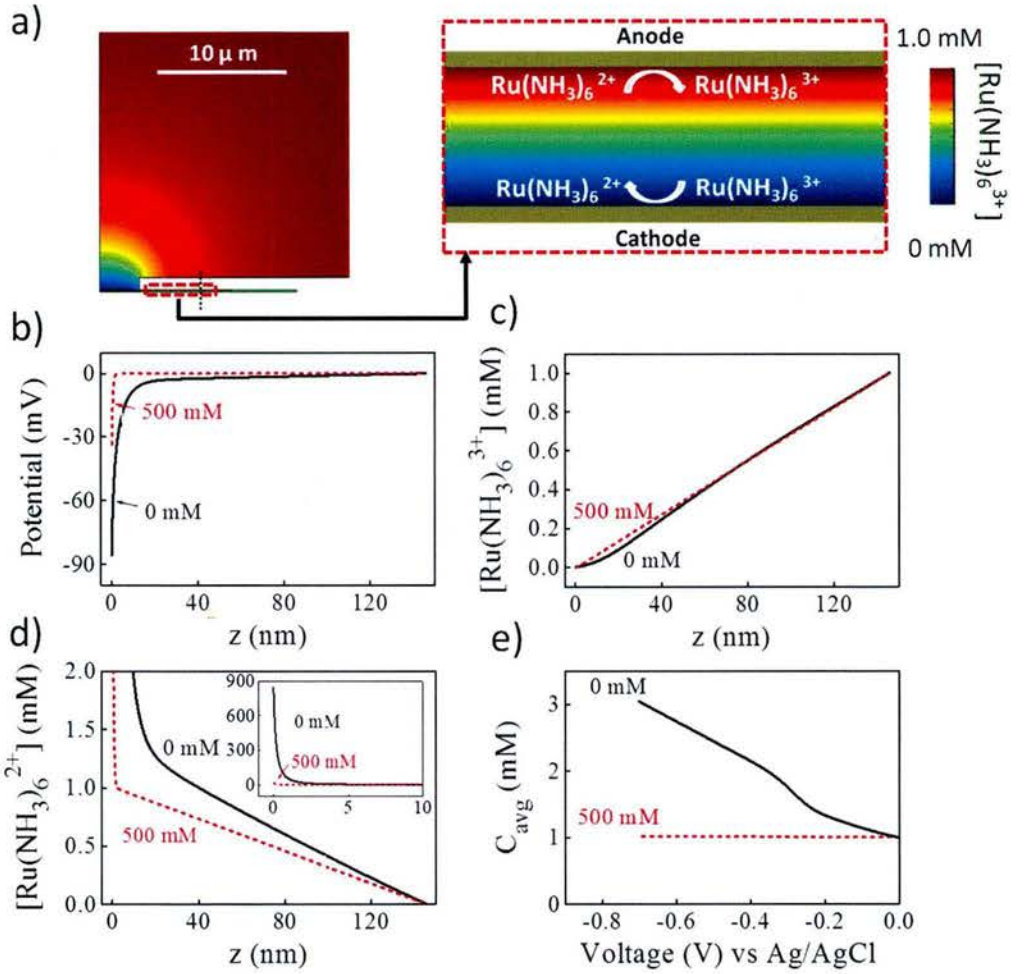

Figure 8. Simulations of 1.0 mM $Ru(NH_3)_6Cl_3$ in a 147 nm thick cell undergoing oxidation at the top electrode (0 V) and reduction at the bottom electrode (−0.7 V). (a) Color plot of the simulated $Ru(NH_3)_6^{3+}$ concentration distribution in the presence of excess supporting electrolyte (500 mM KNO_3) and zoom-in of concentration distribution at the electrode center (red-dashed box). (b) Potential profiles, and (c, d) concentration profiles of $Ru(NH_3)_6^{3+}$ and $Ru(NH_3)_6^{2+}$, respectively, taken across the center of the cell in the same system for 500 mM and 0 mM KNO_3 (along the black dashed vertical line in part a). (e) Total average concentration of redox molecules ($Ru(NH_3)_6^{3+}$ and $Ru(NH_3)_6^{2+}$) between the two electrodes as a function of cathode potential.

The current enhancement was determined to be a strong function of the anode potential, which we can control independently from the cathode potential (see Figure 6). In Figure 9 we see experimental (a&c) and simulated (b&d) voltammograms in the absence of supporting electrolyte and at different anode potentials. In all cases the anode potential is sufficiently positive that the oxidation occurs at a transport limited rate. However, significant current attenuation is observed when the anode is biased positively, whereas when the anode is biased at -0.1 or 0 V, we observe a current enhancement as compared to the diffusion only case (high supporting electrolyte concentration.

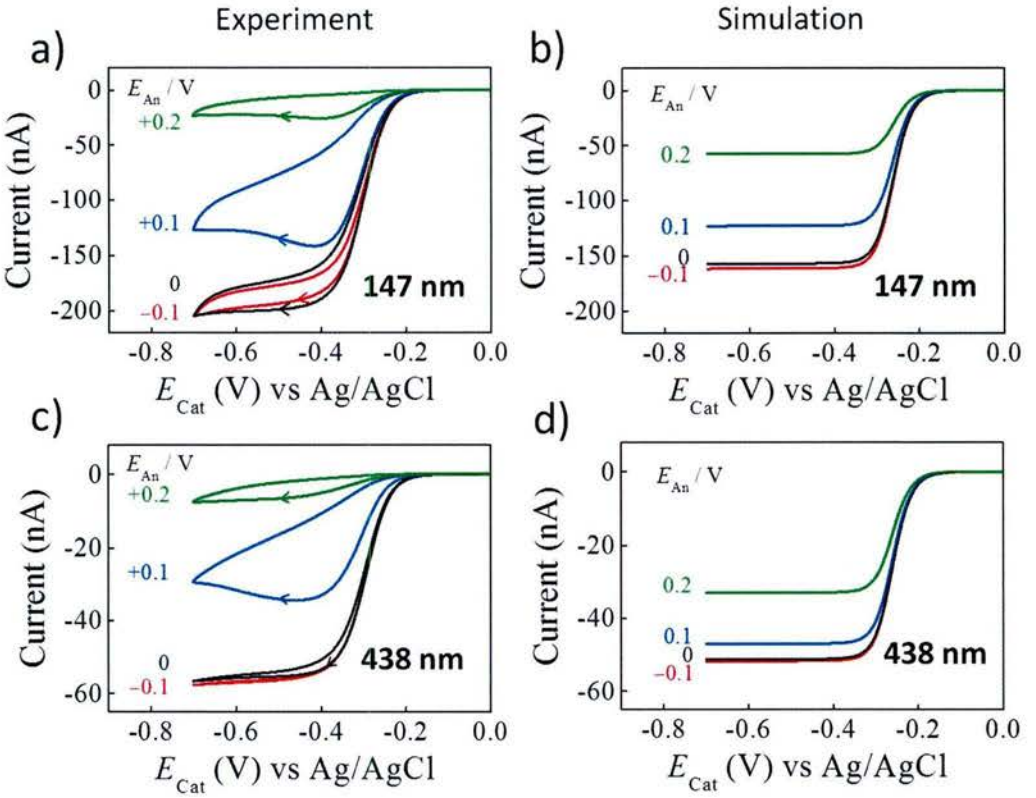

Figure 9. Experimental (a, c) and simulated (b, d) voltammetric responses of 1.0 mM $Ru(NH_3)_6Cl_3$ in H_2O in the absence of KNO_3 at various anode potentials as labeled. Cell thicknesses were respectively (a, b) 147 nm, and (c, d) 438 nm. The scan rate was 10 mV/s. Arrows indicate the direction of forward potential scan.

An understanding of the electrostatic gating of the redox cycling current by the anode potential again required a detailed analysis of the concentration distribution and electric fields between the electrodes, which were obtained through our finite element simulations. We determined that a positive anode potential creates an electrostatic barrier repels $Ru(NH_3)_6^{2+}$ from reaching the anode and causing the dramatic current decrease. These results are reported in a manuscript recently submitted to *ACS Nano.* As noted above, we believe these and previous results have significant impact in understanding the role of electric double layers and ion transport near interfaces in highly confined electrolytes, which are appearing in a range of modern high performance electrochemical energy systems.

Ion- and Electron-Transfer Kinetics at Gas/Liquid/Solid Interfaces: H_2 and N_2 Nanobubbles

Electrochemical and chemical reactions at three-phase interfaces are notoriously difficult to investigate because such boundaries are defined by a very small number of molecules that define the contact line. Nevertheless, three-phase contact lines are very common in electrochemical technologies, e.g., batteries and fuel cells. In the past two years, we initiated an experimental program aimed to develop a fundamental understanding of electron-transfer

reactions at three-phase contact lines and the basic aspects of electrochemical nucleation of new phases. We are developing quantitative techniques for studying *individual* gas bubbles of radius as small as 5 nm defined by *metal/electrolyte/gas* structures. Due to their nanoscale dimensions, the Laplace pressure within these nanobubbles is very high, on the order of ~100 atm. Our measurements are based on low-current electrochemical instrumentation (pico- to nano-amp levels) using metal nanoelectrodes.

In the 2014 EOY report, we described the *first ever* measurements of electron-transfer reaction rates at a single gas/liquid/solid electrode interface [*Langmuir* **2013**, *29*, 11169]. Specifically, we developed an electrochemical approach for investigating the formation and properties of a single nanobubble of with a radius between 5 and 50 nm. At the electrode surface, H^+ in a concentrated acid solution is reduced, creating a supersaturated solution of H_2 adjacent to the electrode surface. As the electrode potential is scanned towards negative potentials, the current arising from H_2 generation increases exponentially and then suddenly decreases to near background levels, signaling a liquid-to-gas phase transformation associated with the formation of a *single* nanobubble at the electrode surface. We measured the critical concentration of dissolved H_2 required for nanobubble nucleation, obtained from a detailed analysis of the electrochemical response, is measured to be ~0.25 M, corresponding to ~310-fold H_2 supersaturation of H_2 [*J Phys Chem Lett* **2014**, *5*, 3539]. Additionally, we demonstrated that nanobubbles can be formed from other gas producing electrochemical reactions in a similar manner, thus validating this methodology as powerful and general tool for investigating electron transfer at three-phase contact lines. We reported the oxidation of hydrazine at Pt nanoelectrodes to create N_2 nanobubbles [*J. Am. Chem. Soc* **2015**, *137*, 12064]. The dependence peak current of electrode radius yields a 160-fold N_2 supersaturation (~0.11 M) necessary to nucleate these bubbles. We also reported electrochemical studies of bubble formation in recessed nanopore electrodes, where the bubble is created in a highly confined space [*Langmuir*, **2015**, *31*, 4573].

i. Electrochemical Measurement of the Lifetime of H_2 and N_2 Nanobubbles

In recent work [*J. Electrochem. Soc.*, **2016**, *163*, H3160-66], we reported the *lifetimes* of individual H_2 and N_2 nanobubbles, electrochemically generated at Pt nanoelectrodes (7 to 85 nm radius), measured using a newly developed fast-scan electrochemical technique, illustrated in Figure 10. To measure the lifetime, a stable single H_2 or N_2 bubble is first generated by reducing protons or oxidizing hydrazine, respectively, at the Pt nanoelectrode. The electrode potential is then rapidly stepped (< 100 μs) to a value where the bubble is unstable and begins to dissolve by gas molecule transfer across the gas/water interface and diffusion. The electrode potential is immediately scanned back to values where the bubble was initially stable. Depending on the rate of this second voltammetric scan, the initial bubble may or may have time to not dissolve, as is readily determined by the characteristic voltammetric signature corresponding to the nucleation of a new bubble. Specifically, at sufficiently fast scan rates, the initial bubble does not dissolve, while at slow scans, the original bubble dissolves and a new bubble is nucleated. The transition between these regimes is used to determine the lifetime of the bubble.

The following theoretical expression describing mixed diffusion/kinetic control was derived and fit to the experimental data to obtain an interfacial gas transfer rate (*h(t)* is the bubble height):

$$\frac{dh}{dt} = -4DRT\left(k_H\left(\frac{4h\gamma}{a^2+h^2} + P_{Ext} \right) - c_b \right) a\Phi(\theta)\left(\frac{\pi}{6} h\left(3a^2+h^2\right)\frac{4\gamma\left(h^2-a^2\right)}{\left(a^2+h^2\right)^2} + \left(\frac{4h\gamma}{a^2+h^2} + P_{Ext} \right)\frac{\pi}{2}\left(a^2+h^2\right) \right)^{-1}$$

The results indicate that dissolution of a H_2 or N_2 nanobubble is, in part, limited by the transfer of molecules across the gas/water interface. These experiments provide the first direct measurement of interfacial gas-transfer kinetic rates for bubbles less than 100 nm in size, and provide a crucial test for existing theories governing bubble dissolution

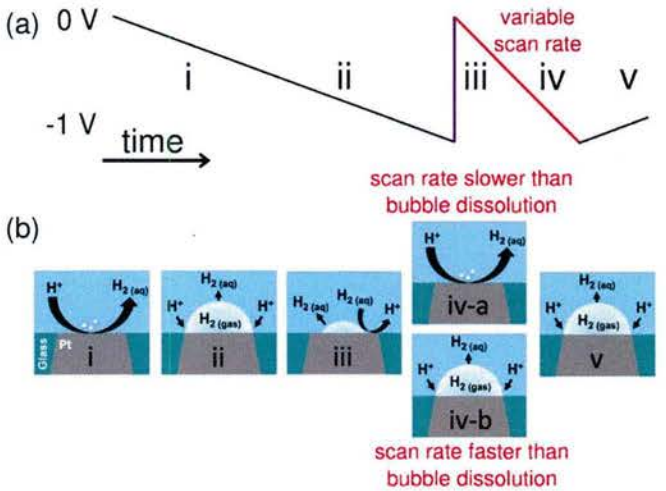

Figure 10. (a) Schematic of the voltammetric experiment used to measure the lifetime of a H_2 nanobubble. The voltage is initially scanned towards negative potentials at 1 V/s resulting in the electrogeneration of H_2 and nucleation (i) of a nanobubble that grows and reaches a dynamic equilibrium (ii). Steps (i) and (ii) result in a voltammetric wave in which the current drops suddenly upon nanobubble formation, as previously shown in Figure 1. At the end of the potential scan (-1V), the electrode potential is stepped back to 0.0 V (iii), a potential at which H_2 is no longer generated, and the H_2 within the bubble is either oxidized to H^+ or diffuses into the bulk solution. A second scan to negative potentials is initiated immediately after the potential step (iv). If the scan rate of this second forward scan is sufficiently slow, the nanobubble has time to completely dissolve, resulting in the nucleation and growth of a new nanobubble on the negative scan (iv-a), which is readily discerned by appearance of the characteristic voltammetric peak for nanobubble formation. Conversely, if the scan rate is sufficiently fast, the preexisting nanobubble does not have time to dissolve.

Figure 11 shows our experimentally measured lifetimes as a function of the nanoelectrode/initial bubble radius (points) alongside predictions of bubble dissolution rates from theoretical models (lines). It is clear that our experimentally measured lifetimes are 1 to 2 orders of magnitude longer than predicted by theory from the literature (solid and dotted lines). Theoretical values were computed both for bubbles that maintain a hemispherical shape during dissolution (as in the Epstein and Plesset model, dotted lines [*J Chem Phys* **1950**, *18*, 1505]), and for bubbles that are initially hemispherical but whose contact line is pinned at the circumference of the initial bubble (as in the Zhang and Lohse model, solid lines [*Phys Rev* E 2015, *91*, 031003]). In the latter case, the bubble radius of curvature increases and, consequently, its internal pressure decreases as it shrinks in height. Both theoretical models assume that bubble dissolution is limited by diffusion and that the dissolved gas concentration at the bubble interface is always at equilibrium with the bubble's internal pressure (determined by its time-dependent radius of curvature) as

described by Henry's Law. Assuming a mass balance during bubble dissolution, where the number of gas molecules leaving the bubble to maintain the surface concentration is compensated by a concomitant change in bubble radius or height by the ideal gas law, allows calculation of the time for the bubble's volume to reach zero. The difference in the assumptions of the two theories yields a prediction of approximately a factor of two slower dissolution for the "negative feedback" model of a pinned bubble relative to the "positive feedback" model of a hemispherical bubble. Both models predict that N_2 bubbles will have lifetimes ~3 times longer than a H_2 bubble of the same size based upon the difference in dissolved gas diffusion coefficients (1.9×10^{-5} cm^2/s and 4.5×10^{-5} cm^2/s for N_2 and H_2, respectively) and difference in gas solubility (0.69 mM/atm and 0.8 mM/atm for N_2 and H_2, respectively).

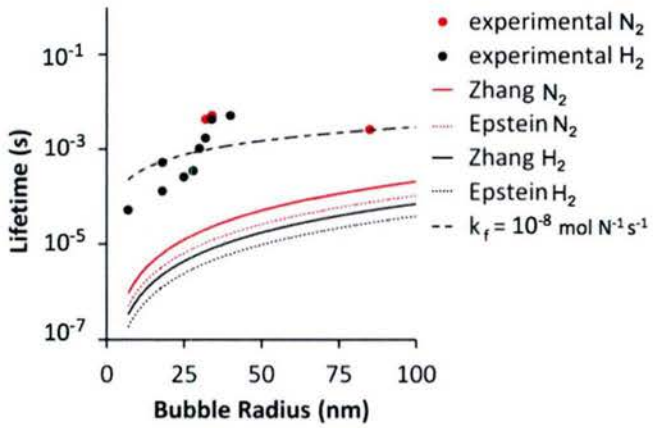

Figure 11. Bubble lifetime *versus* initial hemispherical bubble radius. Black components correspond to H_2 bubbles and red components to N_2. Circles are data points from electrochemical lifetime experiments as shown schematically in Figure 15. Dotted lines are theoretical calculations based upon the model in Epstein and Plesset[*J Chem Phys* **1950**, *18*, 1505] in which bubbles maintain a hemispherical shape as they shrink. Solid lines are theoretical calculations based upon the model in Zhang and Lohse [*Phys Rev E* **2015**, *91*, 031003] in which only the bubble's height shrinks as it dissolves, because its contact line is pinned to the surface. The dashed line incorporates a kinetic rate constant for transfer of H_2 across the gas/water interface to allow a fit to experimental data. From *J. Electrochem. Soc.* **2016**, *163*, H3160

Our measured slower dissolution rates (Figure 11) suggest that a dissolving nanobubble is limited by the transfer of molecules across the gas/water interface. Using the above kinetic equation for dh/dt, a value of $k_f = 1 \times 10^{-8}$ mol N^{-1} s^{-1} provides the best fit to our experimentally determined lifetimes of H_2 bubbles (dashed line, Figure 11). The magnitude of this kinetic constant would have negligible effects on microbubble dissolution rates, because of the reduction in diffusional fluxes at large size bubbles. While the kinetic fit is not particularly compelling, likely due to uncertainties in the experimental system, our results are an intriguing first estimate of interfacial gas transfer limitations at bubbles of nanometer dimensions. To the best of our knowledge, these experiments provide the first direct evaluation of interfacial gas transfer kinetic rates for bubbles less than 100 nm in size.

In summary, we demonstrated a new electrochemical method for the measurement of bubble lifetimes. Studies of H_2 and N_2 nanobubbles show dissolution rates that are ~100 times slower than predictions from extant theories assuming a diffusion-limited process. These

experiments represent an extreme test case where the rate of gas transfer across an interface may not be able to maintain the high equilibrium surface concentration due to the exceedingly fast diffusion of dissolved gas away from the bubble's nanometric gas/water interface.

ii. High-Pressure Electrochemical Measurements of the Laplace Pressure of a Nanobubble

In the past year, we have begun to directly measure the Laplace pressure resulting from interfacial curvature of gas nanobubbles, an experiment that to our knowledge has not been previously achieved, but is of immense current interest in testing thermodynamics relationships at the nanoscale. The surprising longevity of nanobubbles on hydrophobic surfaces and reports of stable nanobubbles in bulk liquid may be an indication that something fundamental related to their thermodynamics is not understood. The idea of a dependence of the surface tension (γ) upon the liquid-gas radius of curvature has been around for decades, yet there currently is no widespread agreement on the length scales at which the curvature becomes important. Guggenheim originally proposed, based upon statistical mechanical considerations, that deviation from values of planar surface tension would begin at curvatures near 50 nm [Trans. Farad. Soc. 1940, *35 397*]. More recently, experimental studies using the surface forces apparatus have demonstrated droplets as small as 4 nm in radius to exhibit a vapor pressure matching the Kelvin equation without modification to the surface tension. [*Nature 1979*, 277, 548] Consensus among theoreticians using molecular dynamics simulations places the transition point for nanodroplets nearer to 1 nm. Castellanos *et al* [*J Phys Chem B 2009, 113,* 5891]. have suggested that bubbles would be expected to behave differently given that they are the inverse morphology of a nanodroplet and argue the transition might be in the micrometer range.

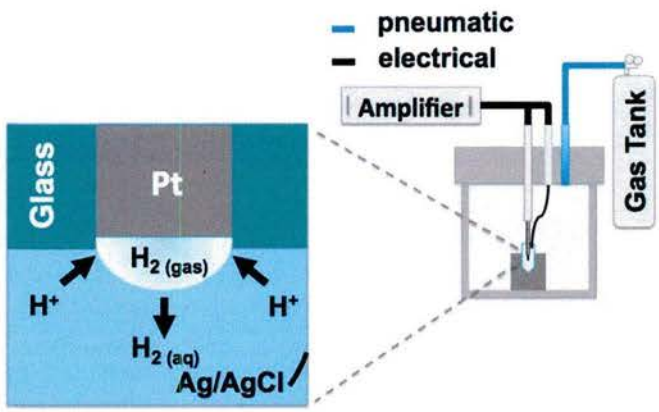

Figure 12. Schematic of custom built pressure chamber designed for electrochemical studies.

This past year, we constructed a novel pressure chamber, Figure 12, to directly measure the Laplace pressure of electrochemically generated nanobubbles as small as 10 nm in radius. Preliminary experiments indicate the residual current after bubble nucleation is *very sensitive* to applied external pressures. We hypothesize that the residual current portion of the voltammogram (the current after stable bubble formation) corresponds to a dynamic equilibrium where the electrogeneration of gas at the 3-phase boundary may be limited by and equal to the outflux of gas away from the bubble surface. The gas solubility increases linearly over the pressure range and as such the flux from the bubble should increase. Schematics of the physics involved are shown in Figure 13. Mathematically, the bubble's internal pressure, P_b, is the sum

of the applied pressure, $P_{external}$, and the radius dependent Laplace pressure,

$$P_b = P_{external} + 2\gamma/r \quad (1)$$

The equilibrium concentration of dissolved gas at the bubble surface, C^s is proportional to the bubble's internal pressure as governed by Henry's Law, k_H.

$$C^s = k_H P_b \quad (2)$$

The flux of dissolved gas away from the bubble surface according to Fick's first law is:

$$J = -D(-C^s/r) \quad (3)$$

Combining Equations 1-3 gives a linear relationship between the residual current and applied pressure:

$$i_r = 2\pi r k_H DnF(P_{external} + 2\gamma/r) \quad (4)$$

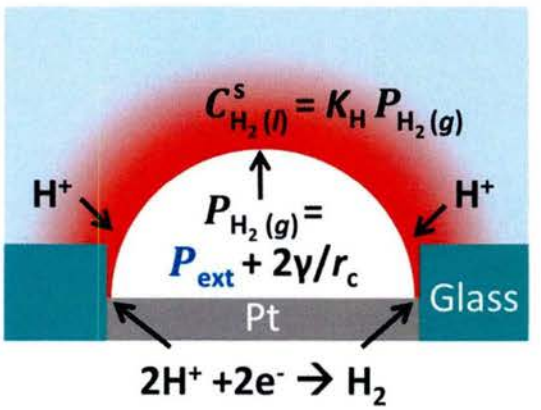

Figure 13. An illustration of the steady-state dynamics of an electrochemically generated nanobubble mathematically described by Equation 4.

Remarkably, Figure 14a shows data from preliminary measurements indicating the residual current does indeed increase precisely as predicted by eq. 4. A plot of the residual current occurring at the 3-phase boundary versus $P_{external}$ is linear and values of γ and the bubble radius of curvature can be determined from the slope and intercept. These preliminary results suggest that the experiment can provide a vast wealth of thermodynamic data that was previously inaccessible to measurements.

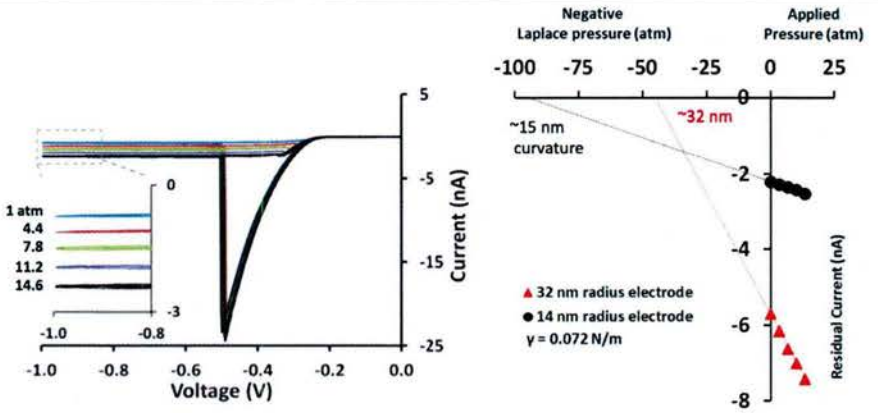

Figure 14. (a) *i-V* response of a hydrogen nanobubble formed at a ~100 nm radius Pt electrode at various applied pressures. With increasing pressure there is a linear increase in the residual current at the 3-phase contact line after bubble nucleation. (b) Extrapolation of the residual current *vs* applied pressure allows calculation of the x-intercept, or negative Laplace pressure ($-2\gamma/r$). The calculated curvature of the bubble using the bulk thermodynamic value for surface tension matches well with the radius of the electrode indicating the bubble is likely hemispherical.

Refereed Journal Articles (All years, 2012-21015)

(1) Petersen, M. K.; Kumar, R.; White, H. S.; Voth, G. A. A Computationally Efficient Treatment of Polarizable Electrochemical Cells Held at a Constant Potential. *J. Phys. Chem. C* **2012**, *116*, 4903–4912.

(2) Xiong, J.; White, H. S. The I-V Response of an Electrochemical Cell Comprising Two Polarizable Microelectrodes and the Influence of Impurities on the Cell Response. *J. Electroanal. Chem.* **2013**, *688*, 354–359.

(3) Luo, L.; White, H. S. Electrogeneration of Single Nanobubbles at Sub-50-nm-Radius Platinum Nanodisk Electrodes. *Langmuir* **2013**, *29*, 11169–11175.

(4) Chen, Q.; Luo, L.; Faraji, H.; Feldberg, S. W.; White, H. S. Electrochemical Measurements of Single H 2 Nanobubble Nucleation and Stability at Pt Nanoelectrodes. *J. Phys. Chem. Lett.* **2014**, *5*, 3539–3544.

(5) Fan, L.; Liu, Y.; Xiong, J.; White, H. S.; Chen, S. Electron-Transfer Kinetics and Electric Double Layer Effects in Nanometer-Wide Thin-Layer Cells. *ACS Nano* **2014**, *8*, 10426–10436.

(6) Cao, Z.; Kumar, R.; Peng, Y.; Voth, G. A. Proton Transport under External Applied Voltage. *J. Phys. Chem. B* **2014**, *118*, 8090–8098.

(7) Chen, Q.; Wiedenroth, H. S.; German, S. R.; White, H. S. Electrochemical Nucleation of Stable N_2 Nanobubbles at Pt Nanoelectrodes. *J. Am. Chem. Soc.* **2015**, *137*, 12064–12069.

(8) Xiong, J.; Chen, Q.; Edwards, M. A.; White, H. S. Ion Transport within High Electric Fields in Nanogap Electrochemical Cells. *ACS Nano* **2015**, *9*, 8520–8529.

(9) Chen, Q.; Luo, L.; White, H. S. Electrochemical Generation of a Hydrogen Bubble at a Recessed Platinum Nanopore Electrode. *Langmuir* **2015**, *31*, 4573–4581.

(10) Feldberg, S. W.; Edwards, M. A. Current Response for a Single Redox Moiety Trapped in a Closed Generator-Collector System: The Role of Capacitive Coupling. *Anal. Chem.* **2015**, *87*, 3778–3783.

(11) Cao, Z.; Kumar, R.; Peng, Y.; Voth, G. A. Hydrated Proton Structure and Diffusion at Platinum

Surfaces. *J. Phys. Chem. C* **2015**, *119*, 14675–14682.

(12) Cao, Z.; Peng, Y.; Voth, G. a. Ion Transport through Ultrathin Electrolyte under Applied Voltages. *J. Phys. Chem. B* **2015**, *119*, 7516-7521.

(13) German, S. R.; Chen, Q.; Edwards, M. A.; White, H. S. Electrochemical Measurement of Hydrogen and Nitrogen Nanobubble Lifetimes at Pt Nanoelectrodes. *J. Electrochem. Soc.* **2016**, *163*, H3160–H3166.

Books And Chapters

- "Electrochemical Double-Layer Effects on Electron Transfer and Ion Transport at the Nanoscale." Wen-Jie Lan, Henry S. White, and Shengli Chen, *in* ***Nanoelectrochemistry, eds.*** Michael V. Mirkin, Shigeru Amemiya, 2015.
-

Technical Reports

-

Contributed Presentations

- "Electrochemistry in Confined Spaces," Gordon Research Conference on Electrochemistry, Ventura, Jan. 2016.
- "Electric Double Layer Effects on Ion Transport in Nanometer Wide Electrochemical Cells," U. of Warwick, UK. July 2015.
- "The electrochemical nucleation and physical behavior of hydrogen nanobubbles," 2015 Electrochemical Society Meeting, Chicago, IL May 2015. *Award Lecture*, Allen J. Bard Award of the Electrochemical Society.
- "Electrical Double Layer Effects on Ion Transport in Thin-Layer Solid-State Electrolytes," American Vacuum Society 62nd Meeting, San Jose, CA. Oct. 2015.
- "The electrochemical nucleation and physical behavior of hydrogen nanobubbles," 2015 Northwest Regional ACS meeting, Pocatello, ID. June, 2015.
- "Electric Field Effects on Ion Transport in a Nanometer Wide Thin Layer Electrochemical Cell", PittCon, New Orleans, FL March. 2015.
-

Patents

-

Honors

-

Related Sponsored Work

2015 Allen J. Bard Award of the Electrochemical Society, Chicago, IL.